Open Access Journal

Journal of Power Technologies 97 (4) (2017) 347–353

journal homepage:papers.itc.pw.edu.pl

Use of 3–dimensional finite elements for computation of temperature distribution in the Stator of an Induction Motor during Direct-On-Line Starting

Nirmal Kr. Bhattacharya[a], Ashok Kr. Naskar[b,*], Debasis Sarkar[c]

[a] *Dept. of Physics, Jadavpur University, Kolkata-32, India*
[b] *Assistant Professor, Dept. of electrical engg., Techno India-Batanagar (TIB), Kolkata-700141, India*
[c] *Professor and Ex-HOD, EE Department, IIEST Shibpur, Howrah-711103, India*

Abstract

Transient thermal analysis of induction machines is a subject of interest for machine designers in their effort to improve machine reliability. Since the stator is static, it is prone to overheating. Therefore, the study of transient thermal behavior in the stator is useful to identify causes of failure in induction machines. This paper presents a three-dimensional transient heat flow through the stator of an induction motor using arch shaped elements in the r-θ-z plane of the cylindrical co-ordinate system. A temperature-time method is employed to evaluate the distribution of loss in various parts of the machine. Using these loss distributions as an input for finite-element analysis, more accurate temperature distributions can be obtained. The model is applied to one squirrel cage Totally Enclosed Fan Cooled (TEFC) machine of 7.5 kW. Finally, the temperatures obtained by this three-dimensional approximation at different locations of the stator were compared for different stator currents considering the time required for each stator current during the transient in Direct-On-Line starting.

Keywords: FEM, Induction Motor, Thermal Analysis, Transients, Design Performance,

1. Introduction

Thermal design is an important consideration at the design stage of induction motors, as it is the thermal problem that is frequently the factor which determines the size and durability of the motor. Thus to design a reliable and economical motor, it is important to produce accurate predictions of temperature distribution within the motor and establish effective use of the coolant to carry away the heat generated in the iron and copper. The heat transfer design is of equal importance as the electromagnetic design of the machine, since the thermal rise of the machine eventually decides its output power.

The problem of temperature rise is twofold: First, in most motors, adequate heat removal is ensured with the thermal convection of air, thermal conduction through the fastening of the machine, and thermal radiation. In machines with high power density, direct cooling methods can be applied as well. In these cases the cooling fluid flows through the machine, removing heat from the interior parts of the machine. Second, the distribution of heat sources has to be considered, i.e., the losses in different parts of the machine. The distribution of heat in the machine can be evaluated when the distribution of the losses in different parts of the machine as well as the heat removal power are exactly known.

Most early designers and researchers traditionally adopted analytical methods such as separation of variables, conformal mapping, and resistance analog networks to predict temperatures. The analytical work is subject to major limitations, alomgside many major assumptions. Even though the resistance analog method predicts average temperatures quite accurately, the method fails to predict hot spot temperatures. Rossenberry Jr. [1] used thermal resistance networks to predict transient stalled temperatures of cast aluminium squirrel cage motors as early as 1955. Chowdhury, S.K et al. [2] presented an exhaustive study on a lumped parameters thermal model for TEFC machines under transient thermal conditions.

The finite difference method is one of the popular numerical methods widely used to estimate core iron and copper winding temperatures in electrical machines [3, 4]. Even though this method predicts hot spot temperatures, the method is not as flexible as the finite element method in handling complex boundary condition and geometry. Use of finite elements [5–10] & [11–21] to solve heat flow has found wide acceptance among researchers in recent years. Rajagopal et al. [22, 23] carried out two-dimensional steady state and transient thermal analysis of TEFC machines us-

*Corresponding author
Email address: naskar73@gmail.com (Ashok Kr. Naskar)

ing the Finite Element Method (FEM). The two-dimensional finite element analysis with analytical lumped-circuit method was introduced recently to predict the temperature rises of two identical prototype surface-mounted permanent magnet machines in a paper by Nannan Zhao et al. [24]. Eddy current distribution in solid magnetic cores was determined using two-dimensional finite element in a paper by Pippuri J.E et al [25].

Taking into account the survey approach of this paper, extensive 3-dimensional analyses have seldom been attempted due to the complexity of the problem and detailed three dimensional transient thermal analyses for hot spot temperature determination in the stator of an induction motor are not known to have been reported for direct-on-line starting of induction motors.

In this paper, the finite element method is used to predict temperature distribution in the stator of an induction motor under transient conditions, using arch-shaped finite elements with explicitly derived solution matrices. Due to the complicated physical geometry of many of the components, the anisotropic nature of the iron laminations, and windings used in the motor, a two-dimensional thermal model cannot represent the problem accurately, especially when one considers the core ends of the motor. Hence, a three dimensional model is used for the analysis. A general derivation of the finite element equations by the method of weighted residuals (Galerkin's method) is introduced. The arch-shaped finite elements are well-suited for electrical machine geometries, and the explicit nature of the solution matrices allows for optimal computer usage. A 100-element 3-dimensional slice of armature iron, together with copper winding bounded by planes at mid-slot, mid-tooth and mid-package, are used to find a solution to a transient heating problem, and this defines the scope of this technique. The computer storage requirements for a large number of elements have been reduced by the use of half band-width of the symmetrical matrices to greatly reduce the computing costs. The model is applied to one squirrel cage TEFC machine of 7.5 kW and the temperatures obtained are found to be within the permissible limit in terms of overall temperature rise computed from the resulting loss density distribution.

2. Finite Element Equations

The general form of the heat conduction equation is:

$$\frac{1}{r}\frac{\delta}{\delta r}(V_r r\frac{\delta T}{\delta r}) + \frac{V_\theta}{r^2}\frac{\delta^2 T}{\delta\theta^2} + V_z\frac{\delta^2}{\delta Z^2} + Q - P_m C_m\frac{\delta T}{\delta t} = 0 \quad (1)$$

Where: V_r, V_θ and V_z are thermal conductivities in the radial, circumferential and axial directions respectively.

2.1. Arch-Element Shape Functions

Consider the arch-shaped prism element of Fig. 1, formed by circle arcs radii a, b, radii inclined at an angle 2α, and prism faces at positions z = -c and z = c.

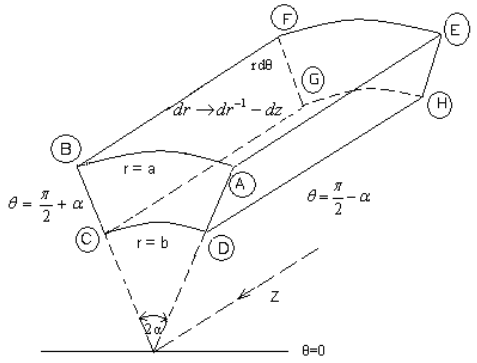

Figure 1: Three-dimensional arch-shaped prism element suitable for discretization of induction motor rotors.

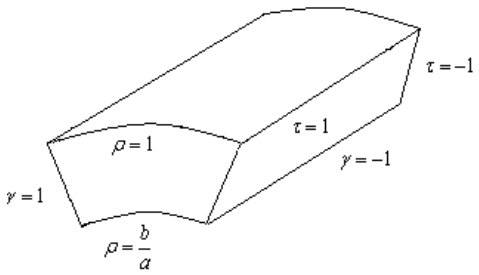

Figure 2: The non-dimensional arch element

The shape functions can now be defined in terms of a set of non-dimensional co-ordinates by non-dimensionalizing the cylindrical polar co-ordinates r, θ and z using;

$$\rho = \frac{r}{a}; \quad v = \frac{\theta - \frac{\pi}{2}}{\alpha}; \quad \tau = \frac{z}{c} \quad (2)$$

The arch element with non-dimensional co-ordinates is shown in Fig. 2.

The temperature at any point within the element be given in terms of its nodal temperatures, by

$$T = T_A N_A + T_B N_B + \cdots + T_H N_H \quad (3)$$

Where: N are shape functions. It is seen that the shape functions satisfy the following conditions:

1. That at any given vertex 'A' the corresponding shape function NA has a value of unity, and the other shape functions NB , NC, . . . , have a zero value at this vertex. Thus at node j, $N_j = 1$ but $N_i = 0$, $i \neq j$.
2. The value of the potential varies linearly between any two adjacent nodes on the element edges.
3. The value of the potential function in each element is determined by the order of the finite element. The order of the element is the order of polynomial of the spatial co-ordinates that describes the potential within the element. The potential varies as a cubic function of the spatial co-ordinates on the faces and within the element.

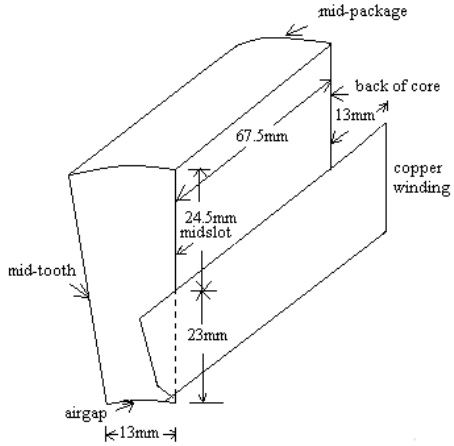

Figure 3: Slice of core iron & winding bounded by planes at mid-slot, mid-tooth.

2.2. Boundary Conditions

In this analysis, the 3-dimensional slice of armature iron and winding chosen for modeling the problem and the geometry is bounded by planes passing through the mid-tooth, the mid-slot and the package center is shown in Fig. 3. The temperature distribution is assumed symmetrical across these three planes, with the heat flux normal to the three surfaces being zero. From the other three boundary surfaces, heat is transferred by convection to the surrounding gas. It is convected to the air-gap gas from the teeth, to the back of core gas from the yoke iron, and to the core end gas from the annular end surface of the core.

2.3. Approximate Numeric Form

The heat flow equation may be formulated in Galerkin's form, the solution being obtained by specializing the general functional form to a particular function, which then becomes the approximate solution sought. There are eight equations for the eight vertices of the element. These equations, when evaluated lead to the matrix equation

$$[[S_R] + [S_\theta] + [S_Z] + [S_T] + [S_H]][T] = [S_T][T_0] + [R] + [S_C] \quad (4)$$

Where: $[S_R]$, $[S_\theta]$ and $[S_Z]$ are symmetric co-efficient matrices (thermal stiffness matrices), $[S_H]$ is the heat convection matrix, $[T]$ is the column vector of unknown temperatures, $[R]$ is the forcing function (heat source) vector, $[S_T]$ is the column vector of heat capacity matrix, $[S_C]$ is the column vector heat convection, $[T_0]$ is the column vector of unknown (previous point in time) temperatures.

3. Application to a Polyphase Induction Motor

The stator of an induction motor, under transient conditions is designed to maintain all temperatures below class A insulation limits of 105°C hot spot. The hottest spot is generally in the copper coils. Thermal conductivity of copper and insulation in the slot are taken together for simplification of calculation [5]. In this analysis, because of symmetry, the three-dimensional slice of core iron and winding, chosen for modeling the problem and the geometry, is bounded by planes passing through the midtooth, the midslot and the package centre, which are divided into finite elements as shown in Fig. 4. Arch-shaped elements are used throughout the solution region. Copper conductors of suitable diameter are embedded in slots to accommodate a slot depth as depicted in Fig. 3. The dimension of the winding included at the end has also been shown in Fig.3. The boundary surfaces, with arch-shaped boundary elements on (i) the tooth tip, (ii) the back of the core surface, and (iii) the annular end surface of the core including the end winding are shown in Fig.4.

Table 1: The natural convection heat transfer co-efficient on cylindrical curved surface over the stator frame

Hydraulic diameter, d, m	0.26
Fluid thermal conductivity, K, W/ m°C	0.0297386
Gravitational acceleration, g, m / s^2	9.8
Reciprocal of film temperature, β, K^{-1}	2.89×10^{-3}
Kinematic viscosity, V, m^2 / s	20.03×10^{-6}
The Grashof number, G_r	80648337
Fluid specific heat, C_p, J / kg°C	1008.344
Fluid dynamic viscosity, μ, kg / m-s	2.06×10^{-5}
The Prandtl number, Pr	0.698
Heat transfer co-efficient, h, W / m^2 °C	5.25

Table 2: The heat transfer co-efficient on forced convection for turbulent flow in cylindrical air-gap surface

Fluid thermal conductivity, K, W / m°C	0.0297386
Hydraulic diameter, d, m	0.165
Fluid density, p, kg / m^3	1.022
Fluid velocity, V, m / s	17.5
Fluid viscosity, μ, kg / m -s	2.06 x 10
Reynolds number, Re,	143253.64
Fluid specific heat, C_p, J / kg° C	1008.344
The Prandtl number, Pr	0.698
Heat transfer co-efficient, h, W / m^2°C	60.16

3.1. Convective Heat Transfer Co-efficient [15, 16]

Three separate values of convection heat transfer co-efficient have been taken for the cylindrical curved surface over the stator frame, the cylindrical air gap surface and the annular end surface.

3.2. Thermal Constants [7]

For a transient problem in three dimensions, the following properties are required for each different material.

Table 3: The heat transfer co-efficient on forced convection for turbulent flow in annular end surface

Fluid thermal conductivity, K, W/m°C	0.0297386
Hydraulic diameter, d, m	0.095
Fluid density, p, kg / m^3	1.022
Fluid velocity, V, m / s	7.5
Fluid viscosity, μ, kg / m-s	2.06 x 10
Reynolds number, Re	35348.300
Fluid specific heat, C_p, J / kg°C	1008.344
The Prandtl number, Pr	0.698
Heat transfer co-efficient, h, W / m^2°C	34.67

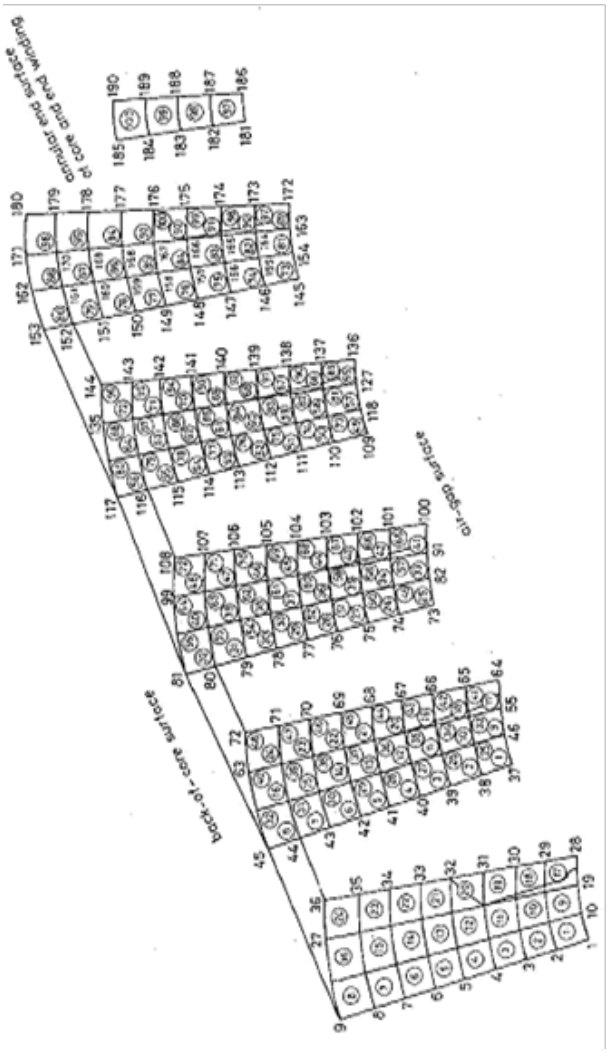

Figure 4: Slice of core iron & winding bounded by planes of mid-slot & mid-tooth divided into arch shaped Finite Elements.

3.3. Calculation of Heat losses

Heat losses in the tooth and yoke of the core are based on calculated magnetic flux densities (0.97 wb/m^2 and 1.293 wb/m^2, respectively) in these regions. Tooth flux lines are predominantly radial and yoke flux lines are predominantly circumferential. The grain orientation of the core punching differs in these two directions and therefore influences the heating for a given flux density. Copper losses in the winding are determined from the length as well as the area required for the conductors in the slot.

- Iron loss in stator core per unit volume = 3.88708×10^{-5} W/mm^3
- Iron loss in stator teeth per unit volume = 3.92352×10^{-5} W/mm^3

3.3.1. A. Stator Copper

The term Direct-On-Line starting as applied to the induction motor refers to the system of starting method in which the stator windings of the motor is excited by rated voltage under D.O.L starting conditions, an induction motor usually requires approximately 6 times its rated current when the rated voltage as applied to the stator. Electromagnetic torque,

Table 4: Typical set of material properties for induction motor stator

	Magnetic Steel Wedge	Copper and Insulation
V_r	33.07	2.007
V_θ	0.826	1.062
V_z	2.874	358.267
P_m	7.8612	8.9684
C_m	523.589	385.361

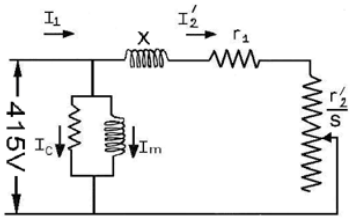

Figure 5: Equivalent circuit on induction motor

$$T_e = \frac{3}{\omega_s} E_t^2 \frac{r_2^{'}/s}{(r_1 + r_2^{'}/s)^2 + (X_1 + X_2^{'})^2} \tag{5}$$

Stator current,

$$I_1 = \sqrt{\frac{T_e \omega_S}{3\frac{r_{I_2}}{s}}} \tag{6}$$

In order to obtain physically operation in the region of slip 0.04<S<1, the current distributions during D.O.L starting condition is calculated using equivalent circuit of Fig. 5 of the machine.

3.3.2. Stator Copper Loss during Transient at different Slips

Stator copper loss = /No. of slots Stator copper loss per slot per unit volume = stator copper loss per slot/ volume of copper Assuming a load of moment of inertia 10 kg-m^2, the time required is calculated at different intervals of speed, i.e., from rest, S=1 to S=0.8 as 3.185 sec to accelerate the motor at a speed of 1440 rpm i.e., 0.96 of the synchronous speed from rest by direct on line starting. The stator currents, stator copper losses per slot per unit volume, Electromagnetic torque and the time required for starting action at different slips in direct-on-line mode are calculated and tabulated in Table 5.

4. Data Analysis

Since the hottest spots are found to be in the stator copper, as envisaged from the calculated temperatures for the three-dimensional structure during the D.O.L starting period, the temperature variation with time at each node of copper

Table 5: The different values of stator current, stator copper loss / slot / unit volume and time required for starting action at different slips in d.o.l starting

Slip	Current, Amp	Electromagnetic torque T_e, N.m	Stator copper loss/slot/unit volume, W/mm^3	Time t_s, sec	Time Δt_s , sec
1	44.738	91.3575	0.0090425	0.0	3.185
0.8	43.338	107.163	0.0084855	3.185	2.694
0.6	40.95	127.574	0.0075761	5.879	2.266
0.4	36.305	150.412	0.0059532	8.145	2.033
0.2	25.632	149.944	0.0029683	10.178	1.524
0.08	12.599	90.569	0.0007171	11.702	0.389
0.06	9.728	71.998	0.0004275	12.091	0.519
0.04	6.658	50.595	0.0002003	12.610	

is taken as an index to understand the temperature profile during the transient. It is to be noted that the temperature is found to be at a maximum at the nodes pertaining to copper in the axis of symmetry. The temperature rise is steady at different stator currents under the D.O.L starting region at slips from s=1 to s=0.4. It is also to be noted that as the motor progresses towards its rated speed there is a slight decrease in hot spot temperatures at a few nodes of copper winding in the axis of symmetry when approaching from the end winding towards the mid-tooth region at slip s=0.2 with a subsequent decrease in hot spot temperatures at all nodes until the motor reaches its rated speed. The temperature variation with time at the hottest spots has been depicted in graphs, as shown in Figs 6–10, to compare the magnitude of the maximum temperature variation with time at various nodal points along the stator copper winding divided into arch shaped elements of length 13.5 mm placed in the axial direction. Finally, the maximum temperatures of the hottest spots along the stator copper winding in the axial direction have been shown in Fig. 11 to signify the nature of variation of the temperature distribution, which follows a definite sequence of nodes in the said region.

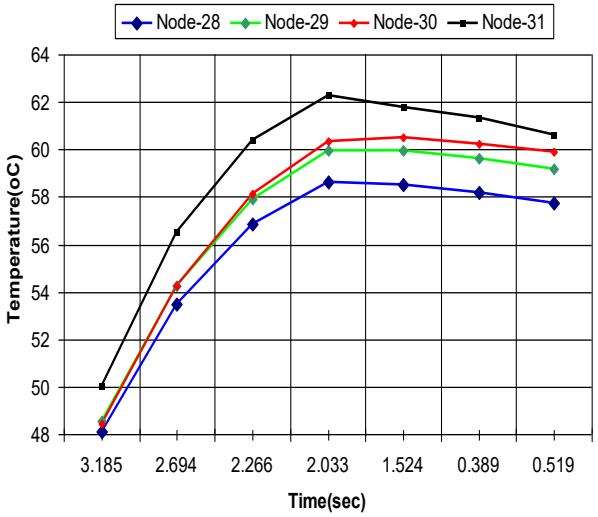

Figure 6: Maximum temperature variation with time at different nodal points along the stator copper winding divided into arch shaped elements of length 13.5 mm

5. Conclusion

In this paper, the three-dimensional transient finite element procedure for the thermal analysis of a Totally Enclosed Fan Cooled (TEFC) squirrel cage induction-motor stator of 7.5 kW under D.O.L starting provides an opportunity for in-depth studies of stator heating problems. By using the new, explicitly derived arch element, together with an efficient bandwidth and Gauss routine, the problem can be solved efficiently. A new three-dimensional finite element procedure in cylindrical polar co-ordinates, with explicitly derived solution matrices, has been applied to the solution of the transient heat conduction equations. This method is fast, inexpensive and leads itself to immediate visual pictures of the temperature pattern in a three-dimensional slice of core iron and winding bounded by planes at mid-slot, mid-tooth and mid-package, divided into arch-shaped finite elements in the stator of an induction motor. This paper is purposed with representing three dimensional transient temperature profiles that are found to be more accurate than the existing model throughout the volume of the stator at selected time intervals during D.O.L starting.

References

[1] G. Rosenberry, The transient stalled temperature rise of cast-aluminum squirrel-cage rotors for induction motors, Transactions of the American Institute of Electrical Engineers. Part III: Power Apparatus and Systems 74 (3) (1955) 819–824.

[2] S. K. Chowdhury, P. K. Baski, A simple lumped parameter thermal model for electrical machine of tefc design, in: Power Electronics, Drives and Energy Systems (PEDES) & 2010 Power India, 2010 Joint International Conference on, IEEE, 2010, pp. 1–7.

[3] K. Reichert, The calculation of the temperature distribution in electrical machines with the aid of the finite difference method, EGZ. A Bd 90 (1969) H6.

[4] C. Tindall, S. Brankin, Loss-at-source thermal modelling in salient pole alternators using 3-dimensional finite difference techniques, IEEE Transactions on Magnetics 24 (1) (1988) 278–281.

[5] A. Armor, M. Chari, Heat flow in the stator core of large turbine-generators, by the method of three-dimensional finite elements part ii: Temperature distribution in the stator iron, IEEE Transactions on Power Apparatus and Systems 95 (5) (1976) 1657–1668.

[6] C.-C. Hwang, S. Wu, Y. Jiang, Novel approach to the solution of temperature distribution in the stator of an induction motor, IEEE transactions on Energy Conversion 15 (4) (2000) 401–406.

[7] A. Armor, Transient, three-dimensional, finite-element analysis of heat flow in turbine-generator rotors, IEEE Transactions on Power Apparatus and Systems (3) (1980) 934–946.

[8] E. Dlala, Comparison of models for estimating magnetic core losses in electrical machines using the finite-element method, IEEE Transactions on Magnetics 45 (2) (2009) 716–725.

[9] S. Ruoho, T. Santa-Nokki, J. Kolehmainen, A. Arkkio, Modeling magnet length in 2-d finite-element analysis of electric machines, IEEE Transactions on Magnetics 45 (8) (2009) 3114–3120.

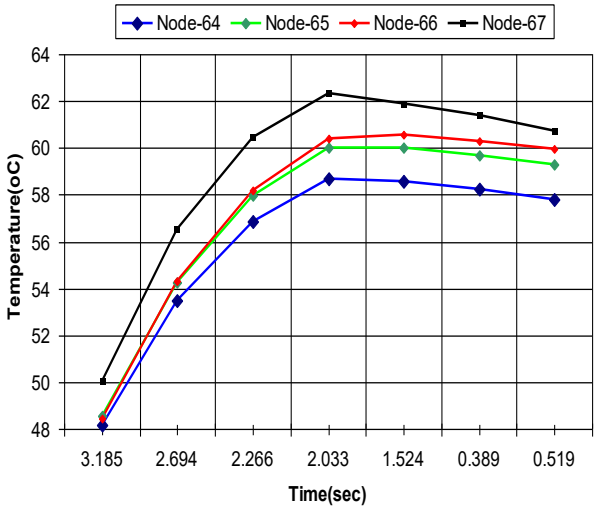

Figure 7: Maximum temperature variation with time at different nodal points along the stator copper winding divided into arch shaped elements of length 13.5 mm

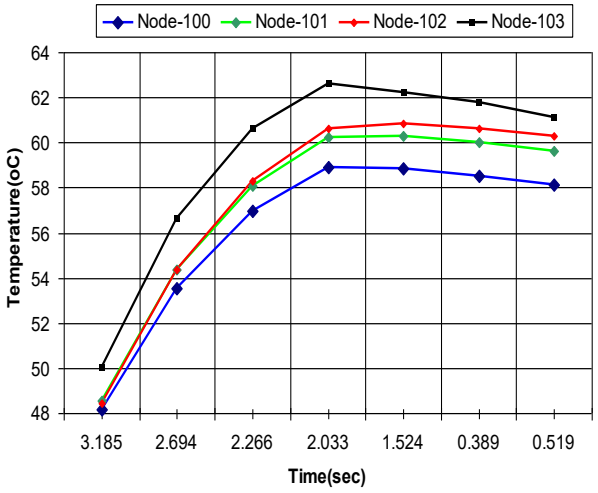

Figure 8: Maximum temperature variation with time at different nodal points along the stator copper winding divided into arch shaped elements of length 13.5 mm

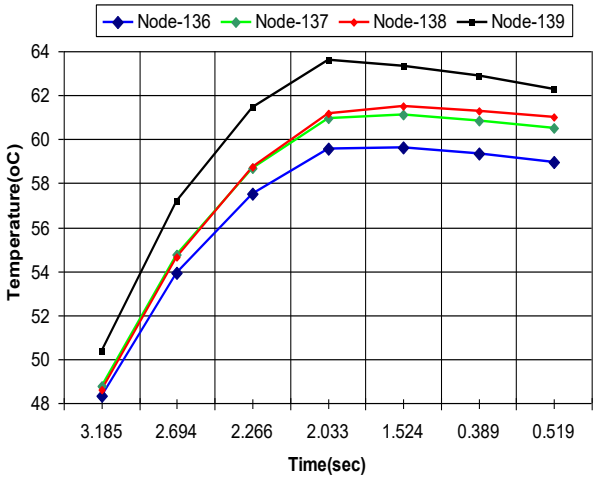

Figure 9: Maximum temperature variation with time at different nodal points along the stator copper winding divided into arch shaped elements of length 13.5 mm

[10] S. Ruoho, E. Dlala, A. Arkkio, Comparison of demagnetization models for finite-element analysis of permanent-magnet synchronous machines, IEEE Transactions on Magnetics 43 (11) (2007) 3964–3968.
[11] H. X. Xia, L. Li, J. J. Du, L. Liu, Analysis and calculation of the 3d rotor temperature field of a generator-motor, in: Electrical Machines and Systems (ICEMS), 2011 International Conference on, IEEE, 2011, pp. 1–4.
[12] M. Islam, A. Arkkio, Time-stepping finite-element analysis of eddy currents in the form-wound stator winding of a cage induction motor supplied from a sinusoidal voltage source, IET Electric Power Applications 2 (4) (2008) 256–265.
[13] R. Lin, A. Arkkio, 3-d finite element analysis of magnetic forces on stator end-windings of an induction machine, IEEE Transactions on Magnetics 44 (11) (2008) 4045–4048.
[14] M. J. Islam, J. Pippuri, J. Perho, A. Arkkio, Time-harmonic finite-element analysis of eddy currents in the form-wound stator winding of a cage induction motor, IET Electric Power Applications 1 (5) (2007) 839–846.
[15] D. AK Sarkar, Naskar, Approximate analysis of transient heat conduction in an induction motor during reactor starting, in: Power Electronics India International Conference, IEEE, 2010, pp. 1–8.
[16] D. Sarkar, N. Bhattacharya, Approximate analysis of transient heat conduction in an induction motor during star-delta starting, in: Industrial Technology, 2006. ICIT 2006. IEEE International Conference on, IEEE, 2006, pp. 1601–1606.
[17] G. B. Kumbhar, S. M. Mahajan, Analysis of short circuit and inrush transients in a current transformer using a field-circuit coupled fe formulation, International Journal of Electrical Power & Energy Systems 33 (8) (2011) 1361–1367.
[18] C. Mejuto, M. Mueller, M. Shanel, A. Mebarki, D. Staton, Thermal modelling investigation of heat paths due to iron losses in synchronous machines, IEEE PEMD.
[19] B. R. Samaga, K. Vittal, Comprehensive study of mixed eccentricity fault diagnosis in induction motors using signature analysis, International Journal of Electrical Power & Energy Systems 35 (1) (2012) 180–185.
[20] R. Mujal-Rosas, Analysis of the three-phase induction motor with spiral sheet rotor, International Journal of Electrical Power & Energy Systems 35 (1) (2012) 1–9.
[21] E. Dlala, Comparison of models for estimating magnetic core losses in electrical machines using the finite-element method, IEEE Transactions on Magnetics 45 (2) (2009) 716–725.
[22] M. Rajagopal, D. Kulkarni, K. Seetharamu, P. Ashwathnarayana, Axisymmetric steady state thermal analysis of totally enclosed fan cooled induction motors using fem, in: 2nd Nat. Conf. on CAD/CAM, 1994, pp. 19–20.
[23] M. Rajagopal, K. Seetharamu, P. Ashwathnarayana, Transient thermal analysis of induction motors, in: IEEE Trans on Energy conversion, Vol. 13, IEEE, 1998, pp. 932–939.
[24] N. Zhao, Z. Zhu, W. Liu, Thermal analysis and comparison of permanent magnet motor and generator, in: Electrical Machines and Systems (ICEMS), 2011 International Conference on, IEEE, 2011, pp. 1–5.
[25] J. Pippuri, A. Belahcen, E. Dlala, A. Arkkio, Inclusion of eddy currents in laminations in two-dimensional finite element analysis, IEEE Transactions on Magnetics 46 (8) (2010) 2915–2918.

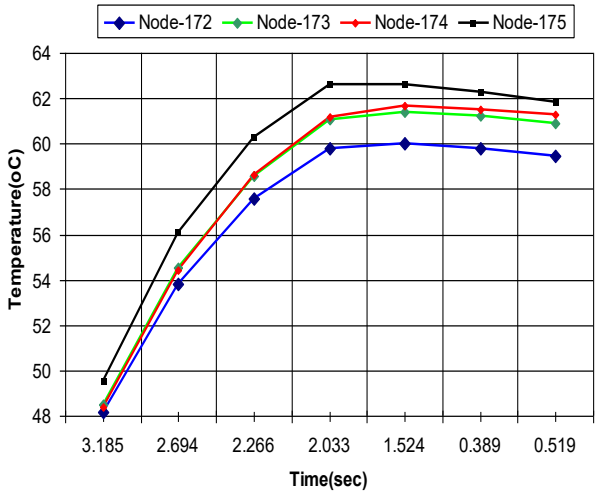

Figure 10: Maximum temperature variation with time at different nodal points along the stator copper winding divided into arch shaped elements of length 13.5 mm

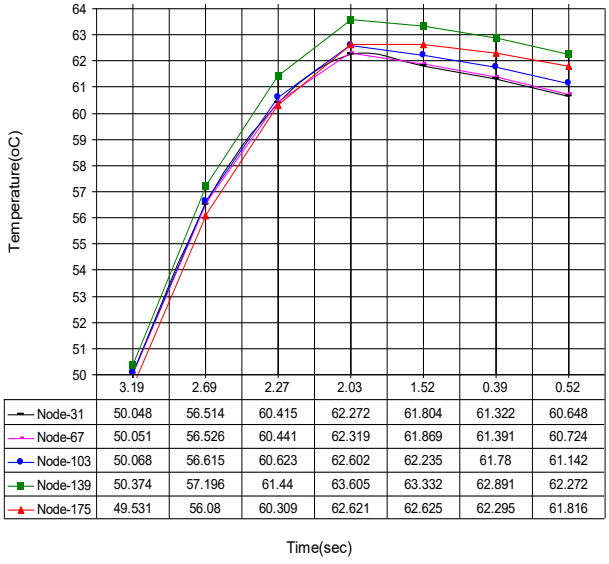

	3.19	2.69	2.27	2.03	1.52	0.39	0.52
Node-31	50.048	56.514	60.415	62.272	61.804	61.322	60.648
Node-67	50.051	56.526	60.441	62.319	61.869	61.391	60.724
Node-103	50.068	56.615	60.623	62.602	62.235	61.78	61.142
Node-139	50.374	57.196	61.44	63.605	63.332	62.891	62.272
Node-175	49.531	56.08	60.309	62.621	62.625	62.295	61.816

Figure 11: Hot-spot temperature variation with time at different nodal points along the stator copper winding